LASER & PHOTONICS REVIEWS
www.lpr-journal.org

Dynamic Transition from Branched Flow of Light to Beam Steering in Disordered Nematic Liquid Crystal

Xiao Yu, Shan-Shan Chang, Zi-Ye Wang, Jiao Liu, Xing-Zhou Tang, Jin-Hui Chen, Bing-Xiang Li,* and Yan-Qing Lu**

Orientational ordered soft matter possessing diverse microstructures has become a focal point of scientific research and technological exploration, thanks to its advancements in serving as an indispensable optical platform enabling propagation of light with multidimensional and manipulatable states. Herein, a facile way is developed to manipulate the in-plane light beam transition dynamics by harnessing a time-variable nematic liquid crystal (NLC) film through the electrical-field-induced topological defects. The results show that the dynamic change of optical branched flow is associated with the growth in the correlation length of optical potential and the reduction in the density of topological defects. The optical branching can continuously transform to deterministic and tunable beam steering at the low-defect-density regime through annihilation kinetics of defects. The explored soft matter system provides an excellent planar platform for the fundamental physics of light interacting with topological defects and may offer new perspectives for novel optics elements toward the applications of soft matter photonics.

1. Introduction

Soft matter, a term first coined by Pierre-Gilles de Gennes in 1991,[1] encompasses materials that lie between aqueous materials and crystalline solids, such as liquid crystals (LCs) and polymers. Soft matter with orientational order exhibits intriguing hierarchical superstructures, formed by the spontaneously self-assembled elementary units, typically LC molecules.[2] Intensively scientific efforts have been directed toward the realization of various patterns with complex orientationally configurations in the soft matter system.[3] This pursuit enables diverse fundamental studies to uncover new properties and effects, as well as technological explorations for new functionalities and applications.[4] Liquid crystals, as an excellent representative, are well-known for their revolutionary applications in the display industry, particularly in liquid crystal displays (LCDs). In LCDs, the director $\mathbf{n}$, which denotes both the average molecular orientation and the optical axis of LCs, is typically reoriented by utilizing an external electric field.[5]

In the early study of the manipulation of director fields, scientists focused on the uniformly oriented LCs where the external field was introduced to collectively reorient the director in a single pixel. These fields could also induce periodic patterns composed of various units, such as rolls and squares, which were demonstrated for use in applications such as optical gratings.[6] Localized patterns of the director distortion, realized in LCs through surface anchoring (photopatterning)[7] and/or external fields,[8] have been widely used in the exploration of light-matter interactions, including the control of optical fields.[7a,9] These mesostructured LC film can be used for laser holography,[10] tunable lens,[11] and microlasers.[10b]

Recently, the topological in-plane steering of light was achieved by LC vortices mimicking the cosmic strings,[12] demonstrating the great potential of light-LC interactions in the planarly transport configuration.[13] When waves travel in a plane of a disordered system, a captivating phenomenon called branched flow emerges.[14] Rather than generating entirely random speckle patterns, the weakly disordered environment fosters focused filaments that intricately divide, resembling the branches of a tree or a river. In recent years, the ubiquitous branched flow effect has been observed in diverse physical systems, such as the initial platform of 2D electron gases,[15] microwaves,[16] sound waves,[17] and water waves.[18] Patsyk et al. recently reported the branched flow of light in thin soap membranes, using the smooth thickness variations of the film as a correlated disordered potential.[19] The unconventional distribution of light intensity associated with the branched flow of light presents opportunities for on-chip light steering and optical diffractive neural networks.[20]

X. Yu, B.-X. Li, Y.-Q. Lu
National Laboratory of Solid State Microstructures
Key Laboratory of Intelligent Optical Sensing and Manipulation
College of Engineering and Applied Sciences
and Collaborative Innovation Center of Advanced Microstructures
Nanjing University
Nanjing 210023, China
E-mail: bxli@njupt.edu.cn; yqlu@nju.edu.cn

X. Yu, Z.-Y. Wang, J. Liu, X.-Z. Tang, B.-X. Li
College of Electronic and Optical Engineering & College of Flexible Electronics (Future Technology)
Nanjing University of Posts and Telecommunications
Nanjing 210023, China

S.-S. Chang, J.-H. Chen
Institute of Electromagnetics and Acoustics
Xiamen University
Xiamen 361005, China
E-mail: jimchen@xmu.edu.cn

The ORCID identification number(s) for the author(s) of this article can be found under https://doi.org/10.1002/lpor.202400366

DOI: 10.1002/lpor.202400366

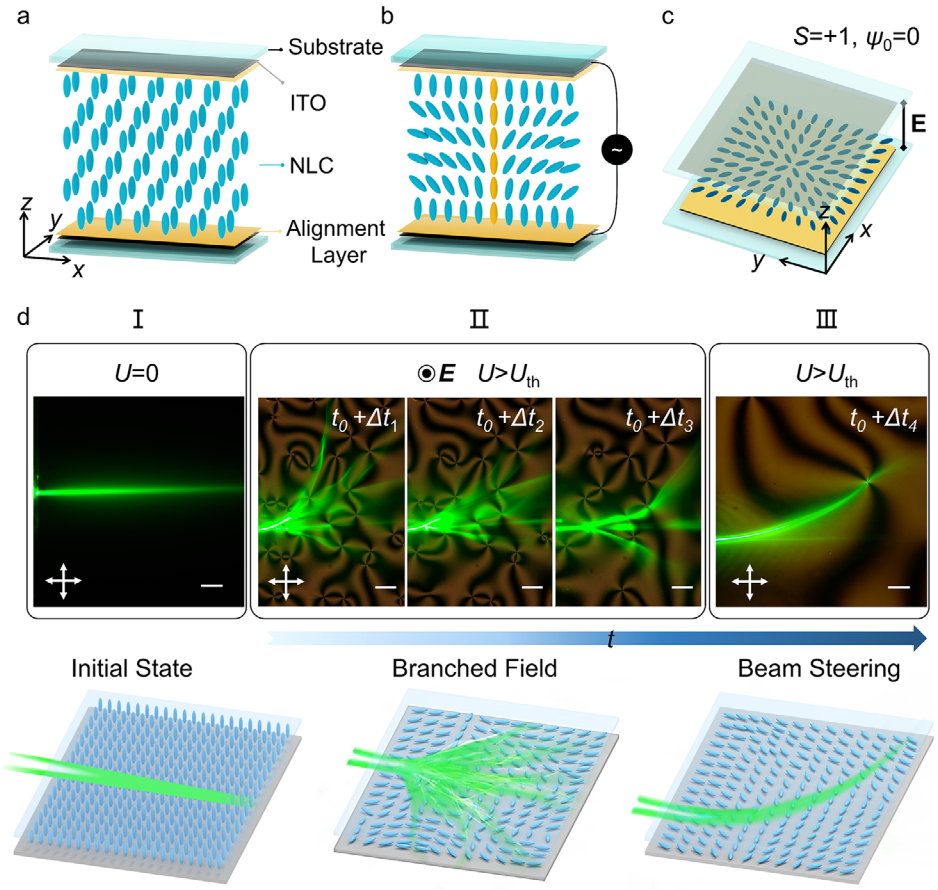

Figure 1. Visualization of branched flow and beam steering in evolving topological structures. a) Schematic diagram illustrates the experimental setup of the nematic liquid crystal (NLC) film with homeotropic alignment. The blue rods represent NLC director. b,c) Schematic illustrates the electrical-field-driven 3D topological structure with oriented director field in x-z plane (b) and x-y plane (c). The orientation of the rods in (c) represents topological defect with topological charge of $S = +1$ and angle constant $\psi_0 = 0$. d) POM images and top-view schematics illustrate the beam propagation in distinct umbilical textures of the NLC under various conditions: (I) Initial state without external electric field $U = 0$, (II) Branched flow of light at any specific time after the application of an AC field with voltage exceeding the threshold ($U > U_{th}$), and (III) Directional beam steering after a prolonged duration (Δt_4) of AC field, ($t = t_0 + \Delta t_4$, $U > U_{th}$). Here, t_0 represents the initial time when the electric field is applied, and Δt_1, Δt_2, Δt_3, Δt_4 represent different duration time of the AC field, satisfying the relationship of $\Delta t_4 > \Delta t_3 > \Delta t_2 > \Delta t_1$. Cross white arrows show the directions of the polarizer and analyzer. Scale bar 200 μm.

In this work, we explore light-matter interactions in an orientationally ordered soft matter system and investigate dynamic transition and manipulation of optical branched flow and beam steering in disordered NLC film by leveraging the inhomogeneous in-plane orientation of the NLC director. The weakly disordered potential is created by using an NLC medium with negative dielectric anisotropy ($\Delta\epsilon < 0$) at high frequency. The mesostructures of NLC are transformed from a uniform and homeotropic alignment to a random planar configuration with various topological defects when the Frederiks threshold is exceeded. Consequently, we achieve reconfigurable branched flow of light by associating the correlation length of the optical potential with the density of topological defects based on the dynamic kinetics of the defects. Moreover, by utilizing the continuous structural transformation of the NLC film and thus the change in optical potential landscapes, we attain the optical transition from branched flow of light to optical steering operating in the low-defect-density regime.

2. Results and Discussion

2.1. Experimental Design

We utilized NLC material (DP002-026, Jiangsu Hecheng Display Technology) with $\Delta\epsilon < 0$ when subjected to a 50 kHz alternating current (AC) electric field at 25 °C. The NLC was infiltrated into a cell constructed of two glass substrates with transparent electrodes through capillary action. These substrates were spin-coated with homeotropic surface alignment layers, aligning the NLC director along the z-axis, $\hat{\mathbf{n}}_0 = (0, 0, 1)$, perpendicular to the $x - y$ plane (**Figure 1a**), as detailed in the Experimental Section. The thickness of NLC cells is $d = 35 \pm 1$ μm. Applying an AC voltage of root-mean-square (rms) value exceeding the threshold voltage $U_{th} = 3$ Vrms, with the electric field normal to the substrates, $\mathbf{E} = (0,0,E)$, induced a Frederiks transition in the homeotropic NLC to an in-plane alignment (Figure 1b).[5] Note that all applied voltages are of frequency 50kHz and their

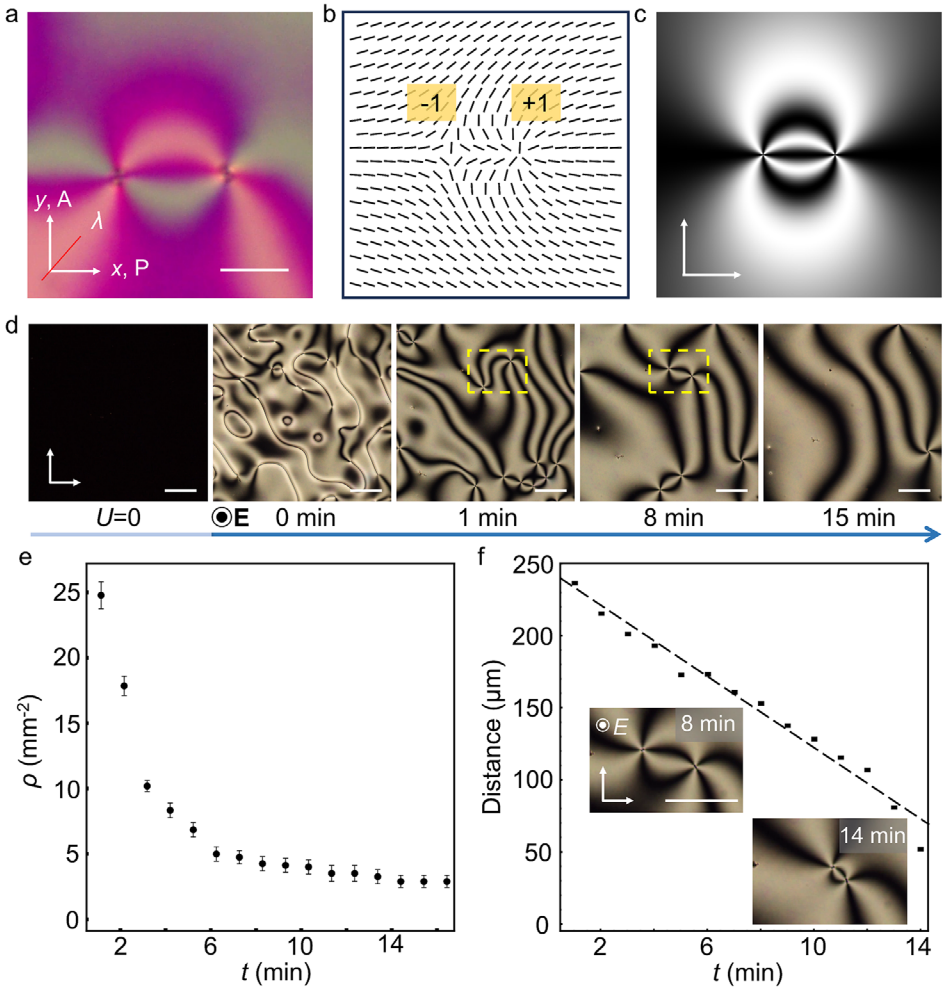

Figure 2. Electrical-field-driven annihilation dynamics of topological defects. a) POM image of a pair of topological defects observed between cross polarizers and a λ-plate. The red line represents the optical axis of the waveplate. Scale bar 200 μm. Schematic director field b) and simulated POM diagram c) of a pair of topological charges of $S = +1$ and $S = -1$, respectively. d) POM images reveal the evolution of topological defects, showcasing the initial state ($U = 0$), Frederiks transition (0–1 min), and subsequent inter-attraction of defects (1–15 min). The gating electric field is $E = 0.6$ V μm^{-1}. The dotted box highlights a pair of topological defects. Scale bar 200 μm. e) Defects density as a function of duration of the electric field. f) Typical time evolution of distance between the defect cores of a pair of defects. The insets are the POM images of NLC topological defects at different time. The dashed black line represents fitting result of linear regression. Scale bar 200 μm.

magnitudes mentioned later are presented with the rms value. Due to the lack of accurate anchoring in the x-y plane, the spontaneous in-plane orientation of the director creates topological defects, which are defined by topological charge S and an angle constant ψ_0. Figure 1c is a top-viewed schematic of the topological defect with $S = +1$ and $\psi_0 = 0$ (Note S1 and Figure S1, Supporting Information). We study the interaction of topological structures with incident linearly polarized light, where the direction of polarization is parallel to the y-direction (Note S2 and Figures S2 and S3, Supporting Information). Note that we utilized a low power of incident light ≈5 mW to avoid the thermal effect and nonlocal nonlinear effect of LC material.[21] In the initial homeotropic state without external stimulation, the laser beam showed an undisturbed trajectory with scattering (Figure 1d-I). Our research demonstrates that the dynamic evolution of topological structures is an excellent platform for tuning the branched flow of light in a disordered NLC film with a high density of defects (Figure 1d-II). Additionally, we have achieved in-plane dynamic beam steering in an NLC film with low-density defects (Figure 1d-III). The optical interaction between the incident light beam and NLC patterns was effectively captured by a specially assembled polarized optical microscope (Figure S4a, Supporting Information), abbreviated as POM, due to cross light scattering during propagation. To record the corresponding NLC texture, we use the scenario of microscopic setup where crossed polarizers and a filter are added (Note S3 and Figure S4, Supporting Information for details).

2.2. Kinetics Annihilation of Topological Defects

The disordered textures of NLC were vividly observed using a cross-polarized optical microscope. A wave plate with

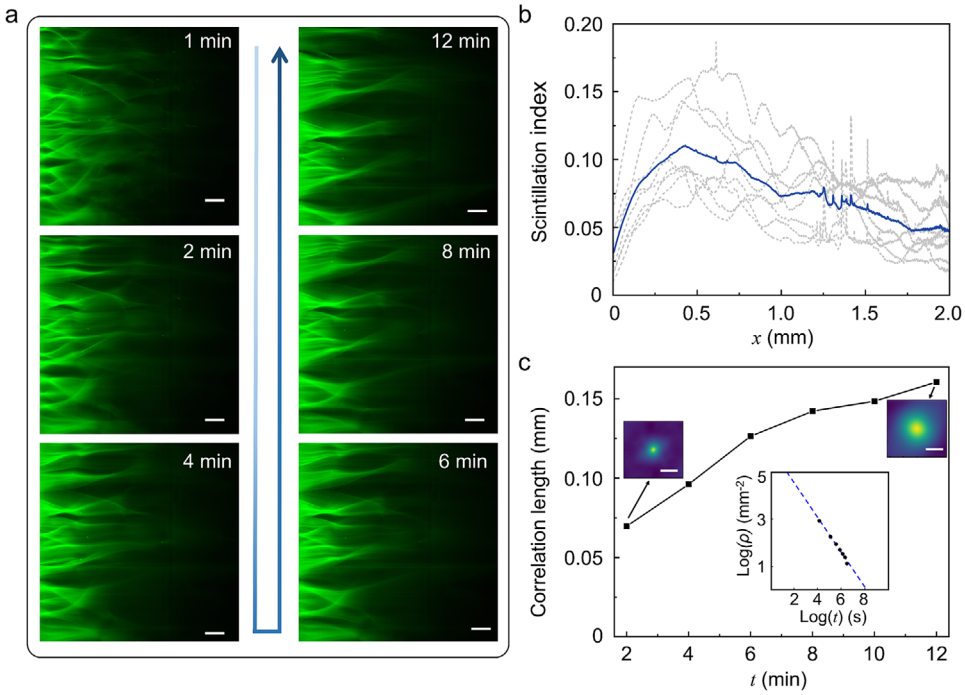

Figure 3. Evolution of branched flow of light in the NLC under quasi-plane-wave incidence. a) Microscope images display the branching field patterns of a broad quasi-plane-wave laser beam propagating in an evolving potential landscape. The driven electric field is $E = 0.3\ \mathrm{V} \cdot \mu\mathrm{m}^{-1}$ over a period of 12 min. b) Scintillation index of propagating optical fields as a function of the propagation distance x. The gray dashed curves represent results extracted from 8 individual measurements at $t = 2$ min, while the blue curve show the average of these 8 realizations. c) Correlation length of optical potentials in the disordered NLC film as a function of the electric field duration, reflecting the evolution over time. Insets illustrate cross sections of the autocorrelation function of the optical potential landscape at ≈2 min and 12 min, respectively. The inset diagram demonstrates the time dependence of defect density, revealing $\rho \propto t^{-1}$. The dashed blue line represents fitting result of linear regression. All the scale bars represent 200 μm.

a wave-length retardation, called λ-plate is added to distinguish the director orientation (**Figure 2a**). This observation revealed two types of topological defects in the director field, similar to schlieren point defects with topological charges of $S = \pm 1$, which are identified as umbilical defects,[22] resembling cosmic strings in their topological nature and evolutionary behavior.[12] The director distribution and polarized geometry of the defect pair can be clearly seen in the simulation (Figure 2b,c). Figure 2d and Figure S5 (Supporting Information) illustrate the evolution of these topological defects, starting from the initial dark field ($U = 0$V), gating voltages ($t = 0$ min), through nucleation ($0 - 1$ min), to mutual annihilation ($t > 1$ min). As shown in Figure 2e, the annihilation of topological defects in NLCs follows a simple scaling law: $\rho \propto t^{-\upsilon}$, where $\upsilon \approx 1$, ρ denotes defect density, and t is the time since the start of the Frederiks transition[22] (Note S4 and Figures S5 and S6, Supporting Information). In this process, the kinetic defect annihilation promotes the evolution of defect density, which can be demonstrated by focusing on the motion of a defects pair. Figure 2f illustrates the relative distance of a pair of defects, where we define the distance as the Euclidean distance between defect cores. The results show that defects approach each other with a uniform speed, $v \approx 0.1\ \mu\mathrm{m\ s}^{-1}$ depicted by the fitted line (Figure 2f). These observed nontrivial topological transformations of NLC can lead to dynamic transitions of in-plane light beam transportation as discussed later.

2.3. Statistic Properties and Dynamic Transformations of Branch Flow of Light

In the branched flow, the statistical properties of wave fields are not determined by the details of the optical potential,[19a] but rather depend on its correlation length l_c and the relative strength of the disordered potentials ϵ. For the electrically gated NLC film, the calculated l_c is on the scale of 100 μm, and ϵ is ≈0.06, thus satisfying the basic requirements for branched flow (Note S5, Supporting Information). More importantly, due to the dynamic transition of topological defects in the electrically gated NLC film and the consequent change in the disordered potential, the transformation of branched flow of light can be observed, as shown in **Figure 3**.

To measure the emergence of the first branching over various potential landscapes, we examined the in-plane transport of light fields using a quasi-plane wave incidence during extended periods of defect annihilation. The quasi-plane-wave light is generated by using a cylindrical lens (Note S2 and Figure S3, Supporting Information). In this configuration, the governing equation of the propagating extraordinary wave (e-wave) in a soft waveguide, created by an NLC film, follows the Helmholtz equation (Note S6, Supporting Information). As shown in Figure 3a, the initially relatively uniform optical fields gradually transition into random caustics featuring high intensity. These random caustics emerge at a propagation distance called the first branching. We observe a decrease in the density of branches over time, which

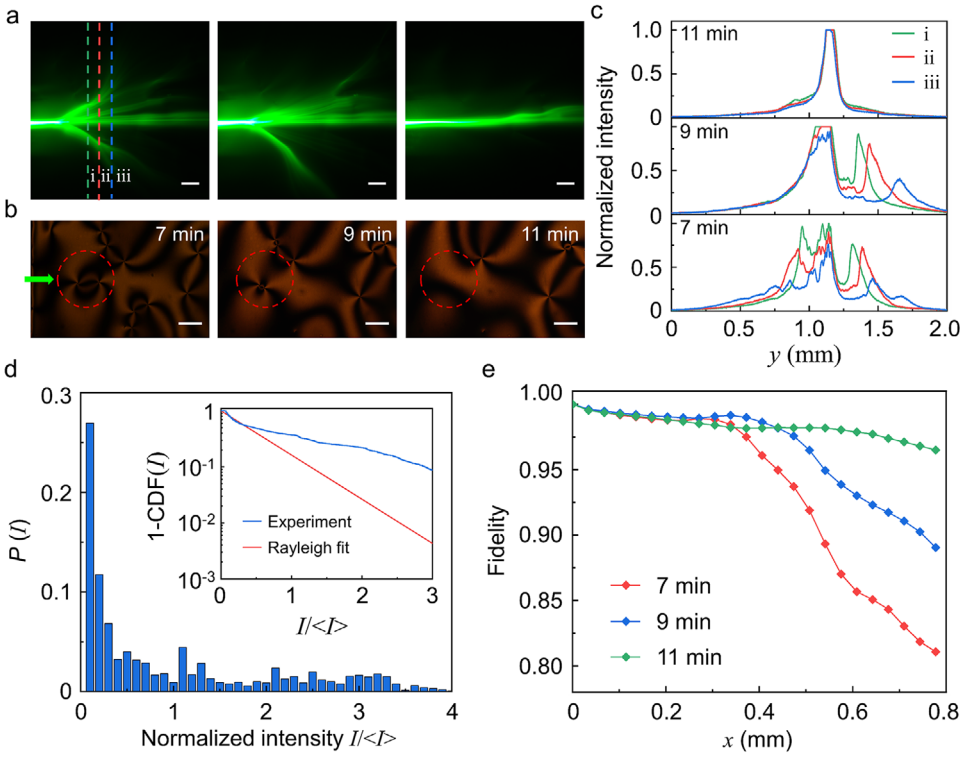

Figure 4. Evolving branched flow of light with Gaussian beam incidence. a) Transitions of in-plane diffraction fields from branched flow patterns (at 7min and 9min) to an approximately non-divergent Gaussian beam (at 11 min) during the defects' annihilation. Scale bar 200 μm. b) POM images depict the annihilation of defects over various evolution times at $E = 0.4$ V μm^{-1}. The initial position of the input beam is marked by a green arrow, and the red dashed circles highlight the defect annihilation process. c) Cross sectional optical field intensity at various transverse positions for different time points. The three panels show the intensity related to the transverse distance ($y-$ axis), taken along the dotted lines in (a). d) Typical probability distribution of branched fields. The statistical data of branched fields are extracted from line position of (ii) in (a) at $t = 7$ min. The inset diagram showcases the cumulative probability of the branched fields (blue curve) exhibiting a heavy tail, in contrast to the Rayleigh distribution (red curve). e) Measured optical field fidelity as a function of propagation distance along the x-axis at different evolution times.

is correlated with the changing potential and the reduction in topological defect density in the LC film.[19] The scintillation index, which quantifies the normalized variance of the optical intensity distribution, is used to evaluate the statistical properties of the branched flow fields (Note S7, Supporting Information). Figure 3b shows the scintillation index of transporting optical fields as a function of the propagation distance for different measurements. To calculate the scintillation index, we average the intensity in each realization over the transverse coordinate. Using the ensemble averaging method, the first branching distance d_f of 0.43 mm can be extracted from the peak position of the average scintillation index curve (blue curve). Based on the statistical length scale of $d_f \propto l_c \epsilon^{-2/3}$,[16,19] the predicted value of the first branching is 0.46 mm under the condition of $\epsilon = 0.058$ and $l_c = 69$ μm, which agrees well with the experimental results.

Intriguingly, we find that the correlation length of optical potentials is monolithically increases with time during periods in the range of $0-12$ min and reaches a saturated value later (Figure 3c). Consequently, the first branching distance should increase with time based on the length scale law $l_c \epsilon^{-2/3}$. Intuitively, the correlation length can be inversely proportional to the topological defect density (Figure 3c; Figure S7, Supporting Information). The distribution of averaging scintillation index (Figure 3b; Figure S8, Supporting Information) revealed a unique peak position in the scintillation distribution at 2 min, with additional peak positions emerging over time. The high-order peak positions gradually merge with the first peak position, leading to a smoothing out of the peaks of the scintillation distribution. This behavior indicates the expansion and movement of the first branching distance observed in the experiment (Figure 3a). However, it is important to note that it is difficult to explicitly extract the shift of the first peak position in the scintillation distribution. This limitation arises from the lack of ensemble measurement data for averaging in dynamic systems. The dynamic evolution of topological structures offers an excellent platform for tuning the branched flow of light in a disordered LC film, which cannot be obtained in previous work.[13,19,23] Moreover, due to its inherent sensitivity to material landscapes, manipulating branched flow offers new perspectives for investigating the transition kinetics of topological defects in the LC film.

The classical scenarios of branched flow can be obtained with a narrow Gaussian beam incident on disordered LC film, as shown in **Figure** 4a (left and middle panels). The light beam splits into different paths after propagating a distance of ≈0.4mm. With the increase in evolving time, the branched flow field patterns fluctuating in a large area are gradually suppressed, since the density of topological defects is significantly reduced (Figure 4b). Under appropriate excitation conditions, the Gaussian beam can

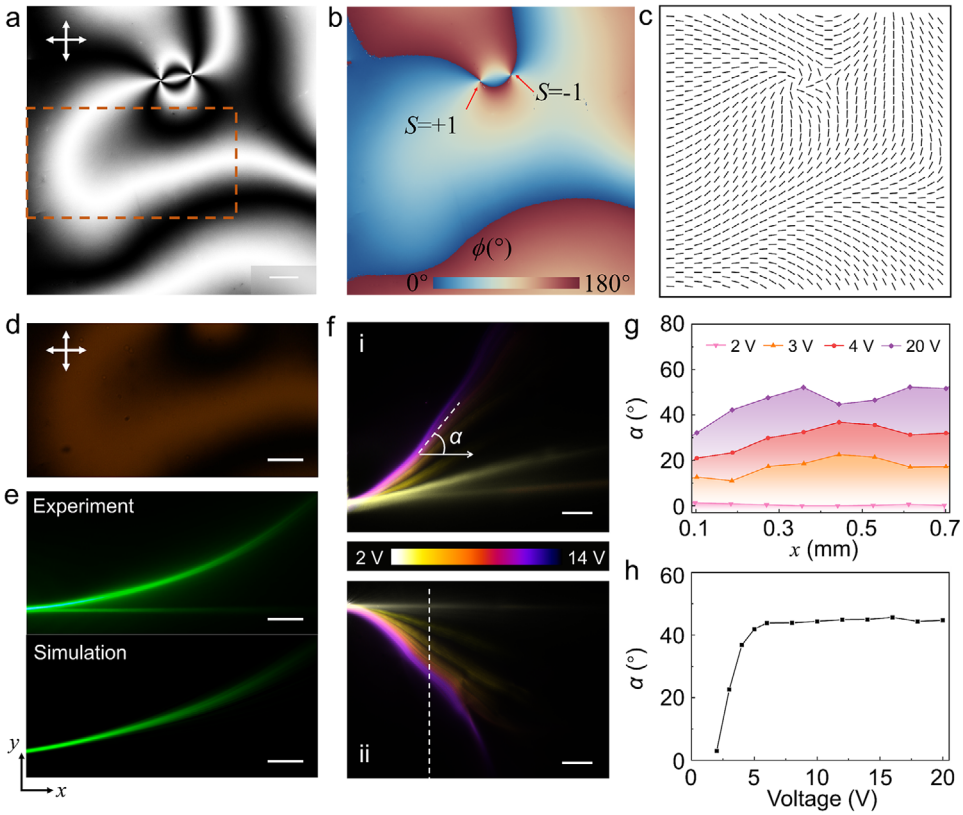

Figure 5. Electrical tuning of beam steering. a) Reconstructed POM image of NLC with ordered distribution of director when subjected to an AC electric field with $f = 50$kHz, $E = 0.4\text{V}/\mu\text{m}$(or $U = 15$ V) for 15 min. Director distribution of the NLC correlated to (a), demonstrated by color-coded diagram b) and rodlike distribution map c). d) POM images of local NLC texture extracted within the dotted rectangle in (a). Scale bar 200 µm. e) Beam steering in the inhomogeneous NLC film. The upper panel shows experimental observations, while the lower panel presents simulations of beam steering corresponding to the conditions in (d). f) Voltage-colored trajectories of optical beam steering. These trajectories demonstrate the electrical tuning of beam bending toward both the $+\gamma$ (i) and $-\gamma$ (ii) directions. Voltages range from 2 V to 14 V, as depicted in the color-coded scheme. Scale bar 200 µm. g) Steering angle (α) of light beam as a function of propagation distance along the x-direction, obtained from light trajectories at different voltages. h) Voltage dependence of α. The α is extracted at $x = 450$ µm as indicated by the dashed white line in (c). All scale bars are 200 µm.

transport over a large distance of 1.2mm, without evident distortion of beam width (Figure 4a right panel), which is similar to light propagation through a homeotropic NLC (Figure 1d-I). During the mutual attraction of defects, branched flow fields are altered as the local director orientation changes, as clearly shown in Figure 4c.

Measuring the probability density of branched flow intensity is crucial for analyzing its unconventional properties. We obtain the cross section light intensity distribution and its probability distribution, as shown in Figure 4d. The cumulative distribution function (CDF) exhibits a pronounced long tail significantly deviating from the Rayleigh function (Figure 4d inset), which is attributed to the formation of high-intensity branches, increasing the occurrence of extreme waves.[19a] To quantitatively characterize the in-plane scattering properties of branched flow, we employ the fidelity parameter to describe the distortions of evolving optical fields (Note S7, Supporting Information). During the evolution process of the LC film with a high density of defects in LC ($t = 7$ min, Figure 4b left panel), the fidelity of propagating fields decays rapidly beyond a traveling distance of ≈0.4 mm. This deflection position is in accord with the theoretical prediction of the first branching. With a further increase in evolution time, the fidelity of transporting optical fields starts to reduce slowly, since the density of topological defects is diminished and the consequent reduction of light scattering.

2.4. Electrical Tuning of the Beam Steering

The dynamic evolution of topological structures in the electrical-field-driven NLC film exhibits a monolithic reduction in defects density as discussed above. **Figure** 5a demonstrates the POM image of the LC film where the defect density is reduced to $\rho = 0.5\text{mm}^{-2}$. Based on the polarization properties of the transmitted light from the NLC (see Experimental Section), we reconstructed the director distribution of the landscape using an optical polarization microscope (Figure 5b,c). The refractive index can be approximately determined from the mapping results of the director under the paraxial approximation (see Note S3, Supporting Information for details). The director distribution progressively organizes itself away from the topological defects (Figure 5d). Consequently, the director distributions present a relatively ordered structure locally in the equilibrium limit. Note that the mesostructured NLC director in Figure 5d is created by applying

an AC voltage of $U = 15$ V for 15 min. By carefully adjusting the incidence position of the excitation light beam along the y-axis, the beam was able to interact with the distant defect, as shown in Figure 5a. In the experiment, we observed deterministic in-plane light beam steering, as illustrated in Figure 5e. The laser beam gets deflected by a defect due to the spatially inhomogeneous distribution of the refractive index (Figure S4, Supporting Information). This bending trajectory is reminiscent of the steering of light by massive celestial bodies like cosmic strings,[12] and it demonstrates a non-spreading parabolic optical path at a propagation distance of ≈1.5mm. The numerical simulation of beam steering can be obtained in Figure 5e lower panel, which agrees reasonably well with the experimental results.

Moreover, we achieve electrically tunable beam steering by simply changing the applied voltages. Due to the negative dielectric anisotropy of NLC, the electric field tends to align the initially out-of-plane director to point along the in-plane. As a result, when the gating voltage is reduced to around the Frederiks threshold, the in-plane aligned NLC molecules start to deflect toward the normal direction. Thereafter, the effective optical potential modulating the beam steering of *e*-wave is weakened and the steering angle of the beam is observed to decreases as the voltage is reduced (Figure 5f). In the Euclidean coordinate system, the steering angle α is evaluated along the propagation distance on the x-axis, as indicated in Figure 5F-i. The beam steering direction can also be reversed by laterally shifting the excitation beam position (Figure 5f-ii). Figure 5g shows the steering angle α of light beams as a function of propagation distance along the x-direction. As anticipated, the overall magnitude of α increases with propagating distance; and by gradually reducing the gating voltages, the angle of steering is consequently decreased. Figure 5h shows that there is a threshold voltage (≈6V) for tuning the bending angle, and this scenario accords to the Frederiks transition.

3. Conclusion

We have demonstrated the in-plane light beam transition dynamics by harnessing a time-variable NLC film. The gating electric field reoriented the initially uniform aligned NLC director, leading to the formation of an in-plane disordered configuration accompanied by topological defects. By utilizing the electrically driven self-evolving disordered potential based on the annihilation kinetics of LC defects, we observed the dynamic transition of light transport from branched flow to deterministic optical beam steering. The deflection of beam steering can be tuned by simply applying voltages of different magnitudes. Our work demonstrates that the explored orientationally ordered system can serve as an excellent platform for studying light transport in disordered media and interacting with topological structures with rich statistical properties, thanks to the electro-optic functions of LC. The dynamic transition of branched flow, as explored in this research, expands a new perspective on the study of transformation kinetics of topological defects in LCs. Furthermore, the optical potential landscapes can be customized using the photo-alignment technique[9] and/or polymerization,[24] offering possibilities for LCs to further manipulate the branched flow of light and develop novel devices for in-plane optical field modulation. We also envision that the independent manipulation of light branches can be achieved by designing specific disordered potential landscapes in LCs[12] or by using wavefront shaping methods.[23] Overall, this research opens up new horizons in the realm of soft matter photonics, offering novel avenues for controlling light in planar structures and advancing diffractive-based optical computing.

4. Experimental Section

Preparation of NLC Sample: The sequence fabrication of a NLC cell is as following. The indium tin oxide (ITO) coated glass plates were ultrasonically cleaned with ethanol, washed with pure water, treated in an ultraviolet ozone equipment to eliminate surface imperfections and remove organic impurities on the surface. After spin-coated with the alignment material NC-M-4070 at 800 rpm for 10 s and 3000 rpm for 30 s, the substrates were placed on a hot plate at 220 °C for 1 h to evaporate the solvent to form homotropic anchoring. Two glass substrates were assembled as an NLC cell by using silica particles embedded Ultraviolet (UV) glue. The size of particles determines the air gap $d = 35 \pm 1$ µm of the cell. The NLC (DP002-026, Jiangsu Hecheng Display Technology) was filled into the empty cell by capillary force at the temperature in the isotropic phase. The NLC DP002-026 exhibits dual-frequency property, where $\Delta\varepsilon > 0$ when $f < f_c$ and $\Delta\varepsilon < 0$ when $f > f_c$. At the temperature of 25 °C for DP002-026, the crossover frequency $f_c = 20$ kHz, $\Delta\varepsilon = -2.8$ at 50 kHz, and the optical birefringence was $\Delta n = n_{//} - n_{\perp} = 0.274$, where $n_{\perp} = 1.511$ was the ordinary refractive index and n_e was the extraordinary one. The temperature of the NLC cell was set by using a hot stage (HCS402XY) and a temperature controller (mK2000B) both purchased from Instec.

Generation and Observation of Topological Defects: The generation of umbilical defects was driven by external electric fields. The NLC cell's glass substrates feature transparent ITO with an active area of 20×20 mm^2. The AC electric field was applied using a waveform generator (33522B, Keysight Technologies Inc.) and an amplifier (ATA-2081, Aigtek). To take the images of topological defects, an illuminating light source was used, a color filter with a central wavelength $\lambda_c = 590$ nm, two crossed polarizers, and a camera.

Realization of the In-Plane Optical Branch Flow and Steering: The light source for the in-plane optical system was a laser of wavelength 532nm (MW-GL-532, Changchun Leishi optical Optoelectronic Technology). The laser beam passes a polarizer, a quarter waveplate, the other polarizer and two lens. Detailed configuration of the setup, see Note S2 (Supporting Information).

Characterization of Azimuthal Angles of the NLC Director: A topological defect could be described through topological charge (S) and angle constant (ψ_0) (Note S1, Supporting Information). The in-plane azimuth angle of the LC directors ϕ with respect to one of the crossed polarizers could be determined by the following two steps: 1) characterizing the topological charge (S) and equivalent azimuthal angle using the polarization properties of light transmitted through LC film; 2) distinguishing the angles constant (ψ_0) of defects using an optical retardance plate. The Jones formalism is commonly used to calculate the propagation of light in the optically uniaxial medium,[25] including NLCs. By applying the Jones matrix of a polarizer in the x-direction, the electric component of transmitting light field could be obtained, expressed as follows:

$$\mathbf{E} = \frac{1}{\sqrt{2}}\begin{pmatrix}10\\00\end{pmatrix}\begin{pmatrix}-i\sin(2\phi)\sin\frac{\Gamma}{2}\\ \sin^2\phi e^{-i\Gamma/2} + \cos^2\phi e^{i\Gamma/2}\end{pmatrix} = \begin{pmatrix}-\frac{i}{\sqrt{2}}\sin(2\phi)\sin\frac{\Gamma}{2}\\ 0\end{pmatrix} \quad (1)$$

where, ϕ represents the angle between the optical axis of the birefringent field (specifically, the director $\hat{n}$ of uniaxial NLC) and x. Γ is the phase retardation between ordinary and extraordinary waves. The retardation is correlated to the sample thickness d, the NLC birefringence Δn, and the light wavelength λ, which can be expressed as $\Gamma = \frac{2\pi}{\lambda}\Delta n \cdot d$. According to formular (1), the intensity of transmitted wave could be obtained:

$$I = \frac{1}{2}\sin^2(2\phi)\sin^2\left(\frac{\Gamma}{2}\right) \quad (2)$$

Since the retardation Γ is correlated to the optical birefringence (Δn) of LC at specific wavelength λ, a quasi- monochromatic light source is required for measurement. The intensity property of the LC texture was captured by synchronously rotating two polarizers (P1 and P2, as depicted in Figure S4, Supporting Information) ranging from 0 to 360 degrees with a constant step $\delta\phi$. It is possible to obtain a sequence of images of a LC defect rotating around a fixed-axis under orthogonal polarizing views. So, the intensity formular could be derived as:

$$I' = \frac{1}{2}\sin^2\left(2(\delta\phi + \phi_0)\right)\sin^2\left(\frac{\Gamma}{2}\right) \quad (3)$$

Here, the light intensity I' of each picture is obtained by extracting the gray value of pixels. The ϕ_0 is the original azimuthal angle of the director that is needed. Using programming software Mathematica 13.0, the method of nonlinear fitting was employed to calculate the angle ϕ_0 for each group of pictures by inputting their respective parameters $\delta\phi$. In the final step, the wave plate with a wave-length retardance was used to determine the angle constant of the defects. It was important to note that in the experiments, the angle constant ψ_0 was determined by comparing the coincidence of the corresponding optical phenomena in both experiments and simulations.

Supporting Information

Supporting Information is available from the Wiley Online Library or from the author.

Acknowledgements

This work was supported by the National Key Research and Development Program of China (Nos. 2022YFA1405000 and 2023YFA1407100), the National Natural Science Foundation of China (Nos. 62375141 and 12274357), the Natural Science Foundation of Jiangsu Province, Major Project (No. BK20212004), Natural Science Foundation of Fujian Province of China (2023J06011), and Fundamental Research Funds for the Central Universities (20720210045). J.-H.C. also thanks the support of Xiaomi Young Talents Program/Xiaomi Foundation.

Conflict of Interest

The authors declare no conflict of interest.

Author Contributions

X.Y. and S.-S.C. contributed equally to this work. X.Y. established the facility and fabricated samples. X.Y. performed the experiments. S.-S.C. built the theoretical model and operated the simulation. X.Y. and S.-S. C. analyzed the results and drew the figures with the help of Z.-Y.W., J.L., X.-Z.T.; J.-H.C., B.-X.L., and Y.-Q.L. organized the paper. B.-X.L. co-supervised the project with J.-H.C. and Y.-Q.L. All authors contributed to the discussion, analyzed the data, and wrote the manuscript.

Data Availability Statement

The data that support the findings of this study are available in the supplementary material of this article.

Keywords

beam steering, branched flow of light, liquid crystals, soft matter photonics, topological defects

Received: March 18, 2024
Revised: May 16, 2024
Published online: June 1, 2024

[1] P.-G. de Gennes, *Angew. Chem., Int. Ed. Engl.* **1992**, *31*, 842.
[2] a) L.-L. Ma, C.-Y. Li, J.-T. Pan, Y.-E. Ji, C. Jiang, R. Zheng, Z.-Y. Wang, Y. Wang, B.-X. Li, Y.-Q. Lu, *Light: Sci. Appl.* **2022**, *11*, 270; b) L. Wang, Q. Li, *Adv. Funct. Mater.* **2016**, *26*, 10.
[3] a) G. Park, Y.-S. Choi, S. J. Kwon, D. K. Yoon, *Adv. Mater.* **2023**, *35*, 2303077; b) Y. Wang, C.-L. Yuan, W. Huang, P.-Z. Sun, B. Liu, H.-L. Hu, Z. Zheng, Y.-Q. Lu, Q. Li, *Adv. Mater.* **2023**, *35*, 2211521.
[4] a) C. Peng, T. Turiv, Y. Guo, Q.-H. Wei, O. D. Lavrentovich, *Science* **2016**, *354*, 882; b) R. Koizumi, D. Golovaty, A. Alqarni, B.-X. Li, P. J. Sternberg, O. D. Lavrentovich, *Sci. Adv.* **2023**, *9*, adf3385; c) M. G. Clerc, M. Kowalczyk, V. Zambra, *Sci. Rep.* **2020**, *10*, 19324; d) L. Huang, X. Chen, B. Bai, Q. Tan, G. Jin, T. Zentgraf, S. Zhang, *Light: Sci. Appl.* **2013**, *2*, 70.
[5] a) P. G. D. Gennes, J. Prost, *The Physics of Liquid Crystals*, Oxford University Press, Oxford **1993**; b) Y.-Q. Lu, Y. Li, *Light: Sci. Appl.* **2021**, *10*, 122.
[6] Y.-L. Li, N.-N. Li, D. Wang, F. Chu, S.-D. Lee, Y.-W. Zheng, Q.-H. Wang, *Light: Sci. Appl.* **2022**, *11*, 188.
[7] a) H. K. Bisoyi, Q. Li, *Chem. Rev.* **2016**, *116*, 15089; b) B.-Y. Wei, W. Hu, Y. Ming, F. Xu, S. Rubin, J.-G. Wang, V. Chigrinov, Y.-Q. Lu, *Adv. Mater.* **2014**, *26*, 1590; c) Y. Guo, M. Jiang, C. Peng, K. Sun, O. Yaroshchuk, O. Lavrentovich, Q.-H. Wei, *Adv. Mater.* **2016**, *28*, 2353.
[8] a) O. D. Lavrentovich, *Liq. Cryst. Rev.* **2020**, *8*, 59; b) H. Zhao, J.-S. B. Tai, J.-S. Wu, I. I. Smalyukh, *Nat. Phys.* **2023**, *19*, 451; c) B.-X. Li, V. Borshch, R.-L. Xiao, S. Paladugu, T. Turiv, S. V. Shiyanovskii, O. D. Lavrentovich, *Nat. Commun.* **2018**, *9*, 2912.
[9] a) P. Chen, B.-Y. Wei, W. Hu, Y.-Q. Lu, *Adv. Mater.* **2020**, *32*, 1903665; b) S.-J. Liu, L. Zhu, Y.-H. Zhang, W. Chen, D. Zhu, P. Chen, Y.-Q. Lu, *Adv. Mater.* **2023**, *35*, 2301714; c) C.-Y. Li, S.-J. Liu, B.-S. Yu, H.-J. Wu, C. Rosales-Guzmán, Y. Shen, P. Chen, Z.-H. Zhu, Y.-Q. Lu, *Laser Photonics Rev.* **2023**, *17*, 2200800; d) K. Yin, E.-L. Hsiang, J. Zou, Y. Li, Z. Yang, Q. Yang, P.-C. Lai, C.-L. Lin, S.-T. Wu, *Light: Sci. Appl.* **2022**, *11*, 161.
[10] a) P. Chen, Z.-X. Shen, C.-T. Xu, Y.-H. Zhang, S.-J. Ge, L.-L. Ma, W. Hu, Y.-Q. Lu, *Laser Photonics Rev.* **2022**, *16*, 2200011; b) L. Chen, Y. Li, J. Fan, H. K. Bisoyi, D. A. Weitz, Q. Li, *Adv. Opt. Mater.* **2014**, *2*, 845.
[11] C. Liu, Y. Zheng, R.-Y. Yuan, Z. Jiang, J.-B. Xu, Y.-R. Zhao, X. Wang, X.-W. Li, Y. Xing, Q.-H. Wang, *Laser Photonics Rev.* **2023**, *17*, 2300274.
[12] C. Meng, J.-S. Wu, I. I. Smalyukh, *Nat. Mater.* **2023**, *22*, 64.
[13] a) T. Wei, P. Chen, M.-J. Tang, G.-X. Wu, Z.-X. Chen, Z.-X. Shen, S.-J. Ge, F. Xu, W. Hu, Y.-Q. Lu, *Adv. Opt. Mater.* **2020**, *8*, 1902033; b) M. Gao, J. Wang, W. Cai, M. Cheng, X. Hao, Y. Wang, Y. Liu, D. Kong, J. Liu, H. Dai, Y. J. Liu, *Nanophotonics* **2023**, *12*, 4205; c) S.-S. Chang, K.-H. Wu, S.-J. Liu, Z.-K. Lin, J.-B. Wu, S.-J. Ge, L.-J. Chen, P. Chen, W. Hu, Y. Xu, H. Chen, D. He, D.-Q. Yang, J.-H. Jiang, Y.-Q. Lu, J.-H. Chen, *Nat. Commun.* **2024**, *15*, 197; d) G. Poy, A. J. Hess, A. J. Seracuse, M. Paul, S. Žumer, I. I. Smalyukh, *Nat. Photonics* **2022**, *16*, 454.
[14] a) E. J. Heller, R. Fleischmann, T. Kramer, *Phys. Today* **2021**, *74*, 44; b) L. Kaplan, *Phys. Rev. Lett.* **2002**, *89*, 184103; c) J. J. Metzger, R. Fleischmann, T. Geisel, *Phys. Rev. Lett.* **2010**, *105*, 020601.
[15] a) M. A. Topinka, B. J. LeRoy, R. M. Westervelt, S. E. J. Shaw, R. Fleischmann, E. J. Heller, K. D. Maranowski, A. C. Gossard, *Nature* **2001**, *410*, 183; b) M. P. Jura, M. A. Topinka, L. Urban, A. Yazdani, H. Shtrikman, L. N. Pfeiffer, K. W. West, D. Goldhaber-Gordon, *Nat. Phys.* **2007**, *3*, 841.
[16] a) S. Barkhofen, J. J. Metzger, R. Fleischmann, U. Kuhl, H. J. Stöckmann, *Phys. Rev. Lett.* **2013**, *111*, 183902; b) R. Höhmann, U.

Kuhl, H. J. Stöckmann, L. Kaplan, E. J. Heller, *Phys. Rev. Lett.* **2010**, *104*, 093901.
[17] M. A. Wolfson, S. Tomsovic, *J. Acoust. Soc. Am.* **2001**, *109*, 2693.
[18] H. Degueldre, J. J. Metzger, T. Geisel, R. Fleischmann, *Nat. Phys.* **2016**, *12*, 259.
[19] a) A. Patsyk, U. Sivan, M. Segev, M. A. Bandres, *Nature* **2020**, *583*, 60; b) A. Patsyk, Y. Sharabi, U. Sivan, M. Segev, *Phys. Rev. X* **2022**, *12*, 021007.
[20] a) T. Fu, Y. Zang, Y. Huang, Z. Du, H. Huang, C. Hu, M. Chen, S. Yang, H. Chen, *Nat. Commun.* **2023**, *14*, 70; b) T. Fu, Y. Zang, H. Huang, Z. Du, C. Hu, M. Chen, S. Yang, H. Chen, *Opt. Express* **2021**, *29*, 31924; c) Y. Huang, T. Fu, H. Huang, S. Yang, H. Chen, *Photonics Res.* **2023**, *11*, 1125.
[21] F. Ye, Y. V. Kartashov, L. Torner, *Phys. Rev. A* **2007**, *76*, 033812.
[22] a) T. Nagaya, H. Orihara, Y. Ishibashi, *J. Phys. Soc. Jpn.* **1987**, *56*, 3086; b) I. Dierking, M. Ravnik, E. Lark, J. Healey, G. P. Alexander, J. M. Yeomans, *Phys. Rev. E* **2012**, *85*, 021703; c) N. Fowler, D. I. Dierking, *ChemPhysChem* **2017**, *18*, 812.
[23] A. Brandstötter, A. Girschik, P. Ambichl, S. Rotter, *Proc. Natl. Acad. Sci. USA* **2019**, *116*, 13260.
[24] a) T. J. White, D. J. Broer, *Nat. Mater.* **2015**, *14*, 1087; b) T. Turiv, J. Krieger, G. Babakhanova, H. Yu, S. V. Shiyanovskii, Q.-H. Wei, M.-H. Kim, O. D. Lavrentovich, *Sci. Adv.* **2020**, *6*, aaz6485.
[25] D.-K. Yang, S.-T. Wu, *Fundamentals of Liquid Crystal Devices*, John Wiley & Sons, Hoboken, NJ, USA **2014**.